

1 **Surface formation, preservation, and history of low-porosity crusts at the**  
2 **WAIS Divide site, West Antarctica.**

3 John M. Fegyveresi<sup>1,2</sup>, Richard B. Alley<sup>2</sup>, Atsuhiko Muto<sup>3</sup>, Anaïs J. Orsi<sup>4</sup>,  
4 Matthew K. Spencer<sup>5</sup>

5  
6 <sup>1</sup>Terrestrial and Cryospheric Sciences Branch, U.S. Cold Regions Research and  
7 Engineering Laboratory (CRREL), Hanover, NH, 03755, USA.

8  
9 <sup>2</sup>Dept. of Geosciences, and Earth and Environmental Systems Institute, Pennsylvania  
10 State University, University Park, PA, 16802, USA.

11  
12 <sup>3</sup>Dept. of Earth and Environmental Science, College of Science and Technology, Temple  
13 University, Philadelphia, PA, 19122, USA.

14  
15 <sup>4</sup>Laboratoire des Sciences du Climat et de l'Environnement, LSCE/IPSL, CEA-CNRS-  
16 UVSQ, Université Paris-Saclay, F-91191, Gif-sur-Yvette, France.

17  
18 <sup>5</sup>School of Physical Sciences, Lake Superior State University, Sault Sainte Marie, MI,  
19 49783, USA.

20

21

22 *Correspondence to:*

23 J. M. Fegyveresi ([fegy.john@gmail.com](mailto:fegy.john@gmail.com); [john.m.fegyveresi@usace.army.mil](mailto:john.m.fegyveresi@usace.army.mil))

24 **Key Words:**

- 25 • Antarctic snow surface, ice cores, field observations, snow-surface crusts, bubble-  
26 free layers, vapor transport, firn properties, snow physics.

27

28

29

30

31

32

## Abstract

33 Observations at the WAIS Divide site show that near-surface snow is strongly altered by  
34 weather-related processes such as strong winds and temperature fluctuations, producing features  
35 that are recognizable in the deep ice core. Prominent “glazed” surface crusts develop frequently at  
36 the site during summer seasons. Surface, snow pit, and ice core observations made in this study  
37 during summer field seasons from 2008-09 to 2012-13, supplemented by Automated Weather  
38 Station (AWS) data with short and longwave radiation sensors, revealed that such crusts formed  
39 during relatively low-wind, low-humidity, clear-sky periods with intense daytime sunshine. After  
40 formation, such glazed surfaces typically developed cracks in a polygonal pattern likely from  
41 thermal contraction at night. Cracking was commonest when several clear days occurred in  
42 succession, and was generally followed by surface hoar growth; vapor escaping through the  
43 cracks during sunny days may have contributed to the high humidity that favored nighttime  
44 formation of surface hoar. Temperature and radiation observations showed that daytime solar  
45 heating often warmed the near-surface snow above the air temperature, which we infer produced  
46 a specific humidity gradient contributing to mass transfer, favoring crust formation and then  
47 surface hoar formation. Subsequent investigation of the WDC06A deep ice core revealed that  
48 crusts are preserved through the bubbly ice, and some occur in snow accumulated during winters,  
49 although not as commonly as in summertime deposits. Although no one has been on site to  
50 observe crust formation during winter, it may be favored by greater wintertime wind-packing  
51 from stronger peak winds, high temperatures and steep temperature gradients from rapid  
52 midwinter warmings reaching as high as  $-15^{\circ}\text{C}$ , and perhaps longer intervals of surface stability.  
53 Time-variations in crust occurrence in the core may provide paleoclimatic information, although  
54 additional studies are required. Discontinuity and cracking of crusts likely explain why crusts do  
55 not produce significant anomalies in other paleoclimatic records.

56 **1: Introduction**

57 Visual and thin-section examination of the WAIS Divide deep ice core from West  
58 Antarctica revealed an annual signal linked to bubble and grain characteristics [Fitzpatrick et al.,  
59 2014], but also numerous crusts. These crusts are bubble-free or nearly so, typically one grain and  
60 1 mm or less in thickness, and are readily identified visually in bubbly ice (Fig. 1). Their presence  
61 in greater abundance than seen in most cores [e.g., Alley, 1988] motivated studies to understand  
62 their formation, possible influence on other paleoclimatic data, and potential for recording  
63 paleoclimatic conditions themselves.

64 Work by Orsi et al. [2015] and Mitchell et al. [2015] showed that no significant artifacts  
65 are introduced to paleoclimatic records by the WAIS Divide crusts. Here, we report additional  
66 studies showing that summertime crusts form under specific conditions linked to persistent high-  
67 pressure systems, so the time-series of crusts likely contains paleoclimatic information; however,  
68 many additional issues must be addressed before useful climate histories could be constructed  
69 confidently.

70 Bubble-free layers much thicker than the bubble-free crusts discussed here are sometimes  
71 observed in ice cores from warm sites, and provide evidence of refrozen meltwater [e.g., Das and  
72 Alley, 2005]. These are of interest as paleoclimatic records but have the potential to anomalously  
73 distort records of trapped gases or other components of ice cores. Refrozen meltwater can be  
74 identified by an excess of trapped heavy noble gases, so Orsi et al. [2015] analyzed WAIS Divide  
75 samples containing bubble-free crusts, finding that not enough meltwater was involved to  
76 significantly perturb records of other trace gases. Additionally, crusts might greatly modify gas  
77 trapping in the firn, but measured nitrogen-isotopic ratios at WAIS Divide show that gravitational  
78 fractionation occurs down to the normal trapping depth where normal amounts of air are trapped,

79 demonstrating that the crusts are not both impermeable and laterally extensive at shallow depth  
80 [Mitchell et al., 2015; Battle et al., 2011].

81 Here, we report coordinated observations of crust formation over five summers (2008-09  
82 to 2012-13) at the WAIS Divide site, involving daily observations of surface evolution, shallow  
83 snow-pit studies with a 2-m pit at least once per year, insolation measurements, and near-surface  
84 temperature profiling, supplemented with data from an on-site automated weather station (AWS).  
85 We find that crusts form most commonly in the summer (45% greater occurrence), but do also  
86 form in winter. In summer, crust formation primarily results from the effects of strong diurnal  
87 temperature cycling under clear-sky, low-wind, relatively warm conditions. Wintertime  
88 observations are not available, but the physical understanding gained from our summertime data  
89 suggests hypotheses for formation. Time-trends in the occurrence of summertime crusts in the  
90 core may reveal changes in the frequency of the persistent high-pressure conditions that generate  
91 crusts, although additional work will be required to quantify this.

## 92 **2: Methods**

93 The main methods used are described here. Additional details are provided in Fegyveresi  
94 [2015]. The surface was observed continually by one of us (JF) during the five field seasons  
95 extending from 2008-09 to 2012-13 (Table 1). During each austral summer, a back-lit snow pit  
96 was also prepared and studied (five total pits). All pits were sited within 1 km radius of the  
97 primary ice-core drilling facility, but avoided regions disturbed by camp operations or the “drift  
98 tail” of enhanced accumulation downwind of the camp. Following prior practice [e.g., Benson,  
99 1962; Koerner, 1971; Alley, 1988], each sampling site involved excavating a pair of ~2 m cubic  
100 pits separated by a wall ~0.5 m thick, with one pit left open to supply back-light, and the other a  
101 roofed observation pit. Features such as crusts and hoar layers were easily identifiable from the

102 observation pit on the back-lit wall (Fig. 2). Pit walls were observed, mapped, sampled, and  
103 photographed (tripod-mounted  $> \frac{1}{4}$  s exposures). Each pit was oriented so the prevailing wind  
104 direction, approximately north-south, ran from right-to-left along the back-lit wall.

105 An automatic weather station (AWS) on site at WAIS Divide (named Kominko-Slade in  
106 the University of Wisconsin AWS system; Lazzara et al. [2012]), collected data on temperature,  
107 air pressure, wind, and humidity starting in the 2009-10 season (all dates and times are GMT).  
108 Beginning in 2011-12, upward-facing and downward-facing short-wave Li-Cor LI200  
109 pyranometers were added initially 1 m above the surface to measure incoming and outgoing  
110 shortwave radiation (0.4-1.1  $\mu\text{m}$  spectral response). Both sensors were newly calibrated and  
111 mounted in a cosine-corrected head (for solar angles up to  $80^\circ$ ), with typical operational errors in  
112 daylight of  $\pm 3\%$  (max  $\pm 5\%$ ). A Kipp-Zonen CNR2 net radiometer with upward- and downward-  
113 facing pyranometers and pyrgeometers was added on an AWS mounting arm during the 2012-13  
114 season, in order to measure both net short- and long-wave radiation. This instrumentation  
115 replaced the previous Li-Cor instrumentation. The pyranometers operated with a spectral  
116 response of 0.3 – 2.8  $\mu\text{m}$ , operational errors of  $\pm 3.5\%$ , and sensitivity of  $15.21 \mu\text{V W}^{-1} \text{m}^{-2}$ , while  
117 the pyrgeometers operated with a spectral response of 4.5–45  $\mu\text{m}$ , operational errors of  $\pm 5.6\%$ ,  
118 and a sensitivity of  $12.52 \mu\text{V W}^{-1} \text{m}^{-2}$  respectively; typical impedances were  $\sim 7$  ohms. All AWS  
119 relative humidity values reported here are expressed in terms of saturation vapor pressure over ice  
120 and corrected for low-temperature offsets (see Anderson, 1994).

121 Also during the 2012-13 season, we calibrated and installed five PRD (platinum  
122 resistance detector) strings in the upper 5 m of firn in a 2 km survey line extending approximately  
123 upwind (grid-west, true-north) starting  $\sim 50$  meters from the on-site AWS. The strings were  
124 designed by one of us (AM) following the procedures in Muto et al. [2011]. Each sensor string  
125 was 5 m long and consisted of 16 individual PRDs (HEL-700 series;  $\pm 0.03^\circ\text{C}$  accuracy,  $\pm 0.18^\circ\text{C}$

126 total combined error, including data-logger error) with denser sampling in the shallower firn to  
127 capture the greater variability there (see also Supplemental Table S2). Sensor calibration took  
128 place over a 60-minute period using a constantly-stirred ice-bath method, and then the newly  
129 calibrated sensors were deployed incrementally over a 10-day period starting Dec. 15<sup>th</sup>.  
130 Deployment boreholes were drilled using a 4 cm diameter hand-auger, and then back-filled once  
131 strings were installed. Campbell logging equipment (CR1000 data logger and AM/16/32  
132 Multiplexer) and 12V sealed lead-acid batteries were housed in a foam-insulated wooden box  
133 beside each borehole and just below the surface. The first string was placed 50 m from the AWS,  
134 and the other strings were placed upwind of it by 10, 100, 1000, and 2000 m (Supplemental Table  
135 S3). Measurements were taken every minute over the survey interval. Each 12V battery was  
136 swapped out weekly with newly charged replacements to ensure that the sensor strings were  
137 continually recording. During each site visit, we took photographs, and noted local  
138 meteorological and surface conditions. Each sensor string took approximately 24 hours to  
139 equilibrate with the surrounding snow following installation due to the backfilling of the open  
140 boreholes with surface snow.

141           We studied crusts in the ice core as well as in the near-surface. As described in  
142 Fitzpatrick et al. [2014], the entire deep core and various associated shallower cores were  
143 inspected visually during core processing lines at the US National Ice Core Laboratory, primarily  
144 by one of us (MS), but with some intercomparisons from other observers. The core was observed  
145 on a light table in a darkened booth, and key features were noted on meter-length log books. The  
146 crusts were easily visible as thin, glassy, bubble-free or nearly bubble-free layers (e.g. Fig. 1).

147           Annual cycles are visible in the bubbly part of the core, arising from the tendency for  
148 near-surface processes to generate coarse-grained, low-density layers including depth hoar in  
149 summer [Fitzpatrick et al., 2014; Fegyveresi, 2015]. However, annual-layer dating of the ice core  
150 using electrical conductivity (ECM, which is primarily controlled by ice chemistry) and soluble-

151 ion chemistry proved more accurate than dating with visible strata [Buizert et al., 2015; Sigl et al.,  
152 2016; WAIS Divide Project Members, 2013]. Here, we estimate the season in which each crust  
153 occurs by assigning each summertime peak in the WD2014 time scale to January 1 of its year, and  
154 then linearly interpolating; accumulation at the site is relatively evenly distributed through the  
155 year, justifying this approximation [Banta et al., 2008; Fegyveresi, 2015, Fegyveresi et al., 2016].

156

### 157 **3: Observations**

#### 158 **3-1: Near-surface observations**

159 We summarize key observations on crust formation here. Additional information, and  
160 complete narrative descriptions of particular crust-forming episodes, are provided in Fegyveresi  
161 [2015].

162 Glazed crusts were repeatedly observed to form on the snow surface (Figs. 3 and 4),  
163 primarily during late-December and January, with an interval between formation events of  
164 roughly one and two weeks (see Figs. 5-8). Crust formation often followed a storm or wind event,  
165 and occurred during a time of higher atmospheric pressure, light winds, clear sky, strong  
166 insolation, large diurnal temperature cycling, and low relative humidity.

167 As shown in Figure 9, the crusts were often internally complex. The upper few  
168 millimeters of firm were anomalously high-density ( $> 400 \text{ kg m}^{-3}$ ) and fine-grained, and might be  
169 termed a multi-grain crust. Within this, and especially at the top, were one or more lower-porosity  
170 single-grain crusts. To an observer, light reflected off these crusts gave the appearance of a glaze  
171 on the snow surface. (e.g. Fig. 4), [see also Orsi et al., 2015, their Fig. 5].

172 Typically, a glazed crust started as isolated sub-meter to few-meter patches on unshaded  
173 regions of the snow surface or sastrugi, which were most consistently exposed to sunlight, and  
174 spaced tens of meters to more than 100 m apart. The spatial size and extent of glazed crusts  
175 varied considerably and were not measured directly, however no single observed crusts patch was

176 greater than 100 m in length in any dimension. Over the first days of formation, glazed crusts  
177 expanded to form a laterally extensive interconnected surface broken by isolated sub-meter to  
178 few-meter unglazed patches on shaded faces of sastrugi. Glazed crusts were most continuous  
179 where the surface was smoothest. Reconnaissance surveys extending a few kilometers from camp  
180 showed that glazed-crust formation was consistent at least that far.

181         Within 2-3 days of formation, glazed features developed prominent polygonal cracks  
182 with few-meter spacing (e.g. Fig. 4). It is likely that these cracks formed by thermal contraction  
183 during nighttime cooling, which was driven by the large diurnal temperature swings observed at  
184 the time (see below). We excavated some cracks, which could be traced downward from the  
185 surface typically ~20-30 cm.

186         A pronounced hoar began forming within 24 hours of the onset of cracking of the glazed  
187 crust in each case observed (e.g. Fig. 3). Measured relative humidity was notably higher during  
188 hoar formation (see Figs. 5-8) than before, and sometimes (e.g., January 7<sup>th</sup>, 2010) a fog  
189 developed early in the time of hoar formation, providing a source of vapor to the surface hoar  
190 from above. Surface glazing was not required for formation of such hoar layers, as one formed  
191 quickly on December 30<sup>th</sup>, 2009 during a very warm ( $> -10^{\circ}$ ) fog episode with elevated measured  
192 relative humidity, but without prior formation of surface glaze.

193         Hoar layers that we observed during the field seasons were subsequently either buried,  
194 destroyed by wind, or gradually sublimated away over 2-3 additional days. We observed strong  
195 winds remove hoar layers, with a threshold of  $\sim 7 \text{ m s}^{-1}$  ( $\sim 13$  knots). In one case, hoar removal  
196 required somewhat lower speed when wind was directed orthogonal to the prevailing direction  
197 and thus sastrugi orientation, similar to observations by Champollion et al. [2013] at Dome C,  
198 East Antarctica.

199         No above-freezing temperatures were observed by the AWS, but on January 2, 2011, the  
200 temperature reached a high of  $-2.8^{\circ}\text{C}$  (see Fig. 6; Supplemental Fig. S1). While no direct surface



201 melt was observed, some melt was noted along exposed, vertically cut wall faces near the ice-  
202 core drilling facility (Supplemental Fig. S2). A prominent multi-grain crust was observed the next  
203 year in snow pits, likely dates from that time, and shows features that are consistent with some  
204 melting-refreezing having occurred (Supplemental Fig. S3).

205         The PRD strings document strong variations in subsurface temperature, following the air  
206 temperatures as expected. During the cooling phases of diurnal cycles, air temperatures (AWS)  
207 and near-surface firn temperatures (S0) dropped well below temperatures deeper in the firn  
208 including the shallowest in-firn sensor (S1) at ~20 cm (Figs. 10 and 11), with the surface as much  
209 as 3°C colder than firn at 40 cm (S2) depth (e.g. Supplemental Fig. S4). This would have driven  
210 upward mass flux from the firn towards the surface. Such conditions often developed when  
211 surface hoar was forming from fog, and thus likely with a downward as well as an upward vapor  
212 source to the near-surface layer.

213

### 214 **3-2: Snow-pit observations**

215         Each of the five snow pits showed a clear annual cycle in the visual stratigraphy, but with  
216 notable “noise”. Depth hoars occurred primarily in summertime layers and into autumn, but with  
217 occasional hoar layers in winter and spring layers. Crusts were also most common in summertime  
218 and into autumn, but not restricted to those times. Similar to the observations made by *Alley*  
219 [1988] at other sites in Antarctica, sequences of strata at WAIS Divide typically showed lateral  
220 continuity over 2 m scales, although with some variation. Many graded beds were also present,  
221 likely indicative of changes during a specific storm event or primarily before the next storm. This  
222 was later confirmed on-site with accumulation stakes and measurements following specific large  
223 storm events (see also Koffman et al., 2014; Criscitiello et al., 2014).

224         The snow pits from the 2008-09, 2009-10, and 2010-11 seasons at WAIS Divide were  
225 mapped here in greatest detail, and meter-wide sub-swaths of their complete pit-wall maps are

226 shown in Fig. 12. Complex stratigraphy and variations are clearly discernable, and illustrate the  
227 variability within 1 km of each other at WAIS Divide in contiguous years. This is likely  
228 indicative of the influence of complex processes of deposition and metamorphism, with frequent  
229 occurrences of depositional and erosional features (sastrugi, whalebacks, wind scoops, hollows,  
230 etc.). We chose annual layers in the pit maps based upon visual inspection in the field,  
231 subsequent examination of photographs of the pits, and overall trends in measured densities (see  
232 e.g. Fig. 13).

233 We measured pit bulk densities using 100 cm<sup>3</sup> stainless-steel, box-type cutters [e.g.,  
234 *Conger and McClung, 2009*] and a digital scale accurate to 1 gram. Density samples were taken  
235 in all five concurrent seasons' pits in duplicate, at ~5 cm intervals, from the pit side-wall (so as  
236 not to disturb the back-lit wall). These duplicates were then averaged together for final values.  
237 Samples measured in the 2008-09 pit were taken with regards to marked strata, and therefore at a  
238 slightly higher frequency. Density measurements from pits of all five seasons yielded an average  
239 density of  $386.6 \pm 3.2 \text{ kg m}^{-3}$  for the upper 2 meters of firn (Fig. 14), all with a nearly identical  
240 linear trend-line slope of  $\sim 0.4 \text{ kg m}^{-3} \text{ cm}^{-1}$  with depth.

241 Seasonal interpretations of all five pits indicated an average of  $\sim 3.75$  years of  
242 accumulation recorded over the 2 meter depths, which yields an average of  $\sim 0.53 \text{ m a}^{-1}$  of  
243 accumulation at the average pit snow-density. Converted to water-equivalent, this becomes  $\sim 0.20$   
244  $\text{m a}^{-1}_{\text{w.e.}}$  (or  $\sim 0.22 \text{ m a}^{-1}_{\text{ice}}$ ). These values agree closely with recently published values (WAIS  
245 Divide Project Members, 2013; Banta et al., 2008; Burgener et al., 2013).

246 We documented obvious crusts and hoar layers for each snow pit. Most commonly, crusts  
247 occurred just above depth hoars, but crusts were observed without hoar, and hoar without crust.  
248 Both single-grain-thick ( $\sim 1 \text{ mm}$ ) and multi-grain ( $\geq 4 \text{ mm}$ ) crusts were observed, with the  
249 common association of single-grain crusts in and usually at the top of multi-grain crusts as noted  
250 above. All crusts had densities estimated over  $400 \text{ kg m}^{-3}$ . Counting a multi-grain crust containing

251 a single-grain crust as one feature, the five 2-meter snow pits revealed an average of  $\sim 18.8 \pm 2.5$   
252 ( $\pm 1\sigma$ ) total crusts, or approximately 5 crusts per year.

### 253 **3-3: Ice-core data**

254 In the bubbly ice included in our crust logging (120-577 m depth) in the WAIS Divide  
255 core, 10,268 crusts were identified (Fig. 15). A few were discontinuous across the core, or  
256 displayed at least a few pores extending through; others appeared largely or completely  
257 continuous and impermeable at the scale of the core. Experience with independent observers  
258 showed little or no error in crust identification. We cannot rule out the possibility that bubble  
259 migration contributed to loss of some crusts in the deepest bubbly ice considered, but the crusts  
260 continued to be clear and readily identifiable, so we do not believe that the trend to fewer crusts  
261 in the deepest ice is an artifact. We cannot fully exclude the possibility that there is an  
262 observational bias related to the drop in crust prevalence over the most recent  $\sim 250$  years, as the  
263 crusts are more difficult to discern in the shallow firn.

264 The seasonal distribution of the crusts is shown in Figure 16. Crusts occur year-round,  
265 but are  $\sim 45\%$  more frequent in summertime accumulation than in wintertime. Certainly, the  
266 natural variability in seasonal distribution of snow accumulation and in the timing of peak  
267 impurity input mean that details of the shape of the seasonal distribution of crust occurrence are  
268 notably uncertain. However, given the high reliability of the annual-layer dating, and the multiple  
269 indicators that agree well [Buizert et al., 2015; Sigl et al., 2016; WAIS Divide Project Members,  
270 2013], “summer” versus “winter” or “nonsummer” are well-constrained.

271 Time-trends of seasonal crust occurrence are also shown in Supplemental Figure S5,  
272 separating the largely sunless winter (May-August) from the sunny spring-summer-fall

273 (September-April, with at least 8 hours of sunlight per day). Both first increase and then decrease  
274 slightly over the 2400-year record, but with a larger relative change in the sunlight season.

275

276

#### 277 **4: Synopsis and Discussion**

278           Our observations confirm and extend prior work on this topic. Depositional processes and  
279 metamorphism primarily in the snow that comprises the upper few centimeters of the firm,  
280 produce prominent layering. Wintertime accumulation, while notably variable, is more  
281 homogeneous than summertime deposits, with wind-packed layers prominent in winter, and  
282 more-variable layers including crusts and hoar more common in summer [e.g., Sorge, 1935;  
283 Benson, 1962, Gow, 1965; 1969; Weller, 1969; Colbeck, 1982; Colbeck, 1983; Alley, 1988;  
284 Alley et al., 1997]. These features are altered during subsequent burial and conversion to bubbly  
285 ice, but still produce recognizable features in the ice core that allow identification of annual layers  
286 and crusts [e.g., Alley et al., 1997; Fitzpatrick et al., 2014].

287           Our observations at WAIS Divide show repeating events that generate the main features  
288 of the summertime accumulation. In a typical event, a storm with strong winds brings snow  
289 accumulation, followed by a high-pressure system bringing clear skies, greatly reduced winds,  
290 initially low humidity, and strong diurnal variations in sunshine, air temperature, and net surface  
291 energy-balance.

292           Early in this clear-sky interval, the wind-packed upper surface develops a millimeter-  
293 thick glazed crust or possibly crusts in a few-millimeters-thick multi-grain crust. Strengthening of  
294 crusts over one to a few days is followed by polygonal cracking from contraction caused by  
295 nighttime cooling. Vapor released through the cracks contributes to rising relative humidity, and  
296 surface-hoar deposition in subsequent nights. At WAIS Divide, evolution of the crust-hoar  
297 complex typically is truncated by arrival of another storm, which may remove or bury the hoar,

298 and typically buries the crusts below the level of fastest metamorphism, allowing them to be  
299 preserved.

300 Not every aspect of a typical event is observed in each case. Crusts form and can be  
301 buried by additional snowfall without growth of a surface hoar on top of them. Crusts are  
302 somewhat discontinuous, and surface hoar can grow where a crust is absent. And, perhaps most  
303 importantly here, a crust that remains near the surface (in the upper few centimeters) for too long  
304 may slowly lose mass and cease to be a crust.

305 Our data provide strong constraints on models of many of the observed processes.  
306 Surface hoar grew especially at night when relative humidity was high, sometimes with fog, and  
307 with deposition occurring on tent ropes or other surfaces as well as on the snow surface (e.g.  
308 Supplemental Fig. S6), clearly demonstrating a source of vapor from above. Surface hoar  
309 typically formed however, when the upper snow surface was colder than layers beneath,  
310 indicating a vapor source from below. Hence, our surface hoars included elements of both  
311 depositional and sublimation hoar crystals as defined by Gallet et al. [2014] based on  
312 observations at Dome C, East Antarctica (with sublimation growth being the dominant process).

313 The high density of both single-grain and multi-grain crusts, approaching the density of  
314 ice for the glassy single-grained crusts, requires that the density of the crusts was increased over  
315 time, as wind packing has not been observed to approach these high densities. Crusts form during  
316 days when atmospheric humidity is low, however, and thus when mass is not being added from  
317 above. We have not observed bulk melting at the site (with the one possible exception noted  
318 above), nor do the gas measurements of Orsi et al. [2015] indicate bulk melting, so the density  
319 increase must arise from some combination of vapor diffusion from below and surface or volume  
320 mass transfer likely involving pseudo-liquid layers [Dash et al., 2006], as discussed next.

321 The data here show that frequently the upper surface is colder than snow beneath, which  
322 will lead to upward mass flux. We lack subcentimetric resolution in thermometry, but physical

323 understanding indicates that very strong gradients likely develop on the centimeter scale just  
324 below the upper surface during rapid nighttime cooling. Physical understanding, the data here,  
325 and data from previously published studies indicate that intense sunshine generates a temperature  
326 maximum in the snow just below the surface (order of 1 cm) especially in low-density, low-  
327 thermal-conductivity depth hoar [e.g., Alley et al., 1990; Brandt and Warren, 1993], also  
328 contributing to upward vapor transport. Hence, the upper surface is expected to gain mass from  
329 below during the crust- and hoar-forming events [Alley et al., 1990]. Windy conditions would  
330 drive undersaturated air into and out of pore spaces, removing mass, but crusts form during  
331 relatively still times. The temperature gradients (and noted inversions) measured here at WAIS  
332 Divide (see also Figures 10 and 11, and Supplemental Figure S4) are similar to those observed at  
333 GISP2 by Alley et al. [1990] and more than sufficient to move the necessary vapor for crust  
334 development.

335         We hypothesize here that these surface conditions cause mass fluxes that fill in open  
336 pores in wind-packed layers at the surface to form glazed crusts. A physical model might be  
337 based on the following considerations. The thermal conductivity of ice greatly exceeds that of air,  
338 so heat transport in firn is primarily conductive. Ordinarily, the grain curvature adjacent to pores  
339 tends to cause diffusive mass loss, enlarging pores by filling necks between grains or other  
340 regions of lower vapor pressure. However, because heat flow is primarily through the grain  
341 structure, pores in a surface crust will tend to be colder than interconnected grains when the upper  
342 surface is colder than the firn beneath, favoring mass transport to the pore surfaces, as shown in  
343 Figure 17 [e.g., Sommerfeld, 1983; Fukuzawa and Akitaya, 1993]. Transport may occur by vapor,  
344 surface, or volume diffusion; following Alley and Fitzpatrick [1999], vapor diffusion and surface  
345 transport in premelted films are likely to dominate. Also, mass loss from relatively warm grain  
346 bonds just beneath a growing surface crust by diffusion to the colder crust will tend to lower the

347 crust, increasing the likelihood that a pore in the crust will move downward to intersect a pre-  
348 existing grain beneath, increasing the crust density.

349         Although summertime crusts dominate in the ice core, many wintertime crusts were  
350 identified, raising additional questions. We lack direct observations in winter, and so can only  
351 speculate on mechanisms active then. However, the basic picture drawn above for summertime  
352 crusts may also apply in winter. The lower temperatures, and lack of intense solar heating, make  
353 crust formation less likely. However, stronger wintertime winds would allow greater wind-  
354 packing of the upper surface, producing fewer and smaller pores to be filled to make a thin crust,  
355 and thus making crust formation easier. Although accumulation is more-or-less evenly distributed  
356 through the year, we speculate (based upon variability observed in AWS data) that there may be  
357 extended intervals up to weeks in length during the winter when the surface is relatively stable,  
358 partially or completely offsetting the slower mass transport from colder temperatures.

359 Furthermore, the AWS data show that mid-winter temperatures have risen as high as  $-15^{\circ}\text{C}$   
360 during strong warming events accompanied by high winds ( $> 10 \text{ m s}^{-1}$ ), and likely linked to  
361 transport of air masses from the coast. Such warm air masses paired with these high winds, would  
362 produce relatively high vapor pressures, contribute to greater surface packing, and promote  
363 temperature inversions and upward near-surface vapor flux during the subsequent cooling.

364         The great abundance of crusts at WAIS Divide compared to other ice cores we have  
365 studied may be because conditions are “just right” at WAIS Divide. We have observed loss of a  
366 wind-packed crust at WAIS Divide, and also at GISP2 in central Greenland; the strong mass loss  
367 from  $\sim 1$  cm down in the snowpack is not conducive to long-term survival of any crust there [e.g.,  
368 Alley et al., 1990]. Low but nonzero summertime accumulation thus may lead to loss of crusts,  
369 whereas higher accumulation after formation buries them below that zone of mass loss and so  
370 allows their preservation. The large wintertime variability and high wintertime temperatures at

371 WAIS Divide may be important in generating sufficiently high mass fluxes to produce wintertime  
372 crusts.

373         At least in summertime, crusts do seem to record a particular meteorological pattern of  
374 storms alternating with still conditions. The time-series of frequency of occurrence of crusts thus  
375 would be affected by a change in the frequency of occurrence of these conditions. Turning this  
376 into a paleoclimatic indicator would require additional steps, however, as the frequency of  
377 preserved crusts could decrease because fewer were formed or because more were destroyed,  
378 with different causes. Information on changing frequency of meteorological events might be  
379 useful [e.g., Hammer, 1985; Alley, 1988]. We believe that the clear association of crust formation  
380 with particular events, and the clear trends in crust occurrence in the core, motivate additional  
381 research on topics including crust formation in non-summer seasons, but we do not know whether  
382 this ultimately could yield a valuable paleoclimatic indicator.

## 383 **5: Conclusions**

384         Summertime observations at the WAIS Divide site show that prominent visible strata  
385 form at or very near the surface during summer, by processes that typically are repeated a few  
386 times during each summer. A storm produces a wind-packed layer. The following high-pressure  
387 system brings light winds, warm days and cool nights, strong sunshine, and low relative  
388 humidity. High-density, single-grain-thick glazed crusts preferentially form at the surface during  
389 these high-pressure intervals, in as little as a single day, and then strengthen and evolve. Crusts  
390 are extensive, although typically broken by sub-meter or few-meter uncrusted regions spaced tens  
391 of meters to more than 100 m apart. Daytime solar heating drives upward mass transport to crusts  
392 from developing depth hoar beneath, strengthening the crusts. After formation, crusts are broken  
393 by polygonal cracks extending typically 20-30 cm deep, likely from contraction during nighttime



394 cooling. Relative humidity then rises in the air above, contributing to growth of surface hoar  
395 during nighttime cooling. Subsequent storms typically bury the crust-hoar complexes, although  
396 crusts can be lost during evolving surface conditions if not buried below the top one to a few  
397 centimeters.

398 Study of the WAIS Divide deep core shows that crusts are preserved through the bubbly  
399 ice. Crusts are most common in layers deposited during summertime, but also occur in winter  
400 accumulation. Study of AWS data suggests that the intrusion of warm coastal air during winter  
401 may generate strong temperature gradients, which may contribute to wintertime crust formation  
402 in wind-packed layers.

403 The frequency of occurrence of crusts in the core varies with time, suggesting the  
404 possibility that crusts could be used as a paleoclimatic indicator. However, additional work  
405 would be required, including addressing whether crust frequency varies because of changes in  
406 formation or changes in destruction of crusts previously formed. The crusts do not produce  
407 significant anomalies in other ice-core paleoclimatic records, likely at least in part because they  
408 are discontinuous and broken by contraction cracks.

#### 409 **6: Data Availability:**

410 Data policy: All data presented here are available via download from NSIDC  
411 (<http://nsidc.org>) or from the WAIS Divide data portal (<http://waisdivide.unh.edu>).

412

#### 413 **7: Author Contribution:**

414 A.J. Orsi assisted with field observations and experiments. A. Muto designed the near-  
415 surface PRD sensor strings and developed the associated logging code. M. Spencer documented

416 all ice-core crust observations during the WAIS Divide core processing at the National Ice Core  
417 Laboratory. J.M. Fegyveresi and R.B. Alley prepared the manuscript with contributions from all  
418 co-authors.  
419

420 **8: Acknowledgements:**

421           We acknowledge the following funding sources for support of this work: U.S. National  
422 Science Foundation Division of Polar Programs grants 0539578, 1043528, 1142085, 1619793.  
423 We also acknowledge Donald E. Voigt, Joan J. Fitzpatrick, Eric D. Cravens, and the staff of the  
424 U.S. National Ice Core Laboratory in Denver, Colorado, as well as the WAIS Divide Science  
425 Coordination Office at the University of New Hampshire, and the Ice Drilling Design and  
426 Operations group at the University of Wisconsin. We thank numerous colleagues involved with  
427 the WAIS Divide project, especially Kendrick Taylor, Mark Twickler, and Joseph Souney. We  
428 thank Bess Koffman, Gifford Wong, Dominic Winski, Aron Buffen, and Logan Mitchell for  
429 assistance with snow pit preparation. Lastly we thank Jonathan Thom and the University of  
430 Wisconsin-Madison Automatic Weather Station Program for assistance with weather station  
431 sensor installation. Any use of trade, firm, or product names is for descriptive purposes only and  
432 does not imply endorsement.

433

434

435 **9: References**

- 436 Alley, R.B., 1988. Concerning the deposition and diagenesis of strata in polar firn. *Journal of*  
437 *Glaciology*, 34: 283-290.
- 438 Alley, R.B., Saltzman, E.S., Cuffey, K.M. and Fitzpatrick, J.J., 1990. Summertime formation of  
439 depth hoar in central Greenland. *Geophysical Research Letters*, 17(13): 2393-2396,  
440 doi:[10.1029/GL017i013p02393](https://doi.org/10.1029/GL017i013p02393).
- 441 Alley, R.B. and Fitzpatrick, J.J., 1999. Conditions for bubble elongation in cold ice-sheet ice.  
442 *Journal of Glaciology*, 45(149): 147-153.
- 443 Alley, R.B., Shuman, C.A., Meese, D.A., Gow, A.J., Taylor, K.C., Cuffey, K.M., Fitzpatrick, J.J.,  
444 Grootes, P.M., Zielinski, G.A., Ram, M. and Spinelli, G., 1997. Visual-stratigraphic  
445 dating of the GISP2 ice core: Basis, reproducibility, and application. *Journal of*  
446 *Geophysical Research: Oceans*, 102(C12): 26367-26381, doi:[10.1029/96JC03837](https://doi.org/10.1029/96JC03837).
- 447 Anderson, P.S., 1994. A method for rescaling humidity sensors at temperatures well below  
448 freezing. *Journal of Atmospheric and Oceanic Technology*, 11(5), 1388-1391.
- 449 Anderson, D. L., and Benson C.S., 1963, The densification and diagenesis of snow, in *Ice and*  
450 *Snow: Properties, Processes and Applications*, edited by W. D. Kingery, pp. 391–411,  
451 MIT Press.
- 452 Banta, J.R., McConnell, J.R., Frey, M.M., Bales, R.C. and Taylor, K., 2008. Spatial and temporal  
453 variability in snow accumulation at the West Antarctic Ice Sheet Divide over recent  
454 centuries. *Journal of Geophysical Research: Atmospheres*, 113(D23), doi:  
455 [10.1029/2008JD010235](https://doi.org/10.1029/2008JD010235).
- 456 Battle, M.O., Severinghaus, J.P., Sofen, E.D., Plotkin, D., Orsi, A.J., Aydin, M., Montzka, S.A.,  
457 Sowers, T. and Tans, P.P., 2011. Controls on the movement and composition of firn air at  
458 the West Antarctic Ice Sheet Divide. *Atmospheric Chemistry and Physics*, 11(21), 11007-  
459 11021, doi:[10.5194/acp-11-11007-2011](https://doi.org/10.5194/acp-11-11007-2011).
- 460 Benson, C.S., 1962. Stratigraphic Studies on Greenland Ice Sheet and a Quantitative  
461 Classification of Glaciers. *Bulletin of the American Meteorological Society*, 43(4): 141.
- 462 Brandt, R.E. and Warren, S.G., 1993. Solar-heating rates and temperature profiles in Antarctic  
463 snow and ice. *Journal of Glaciology*, 39(131), 99-110.
- 464 Buizert, C. et al., 2015. The WAIS Divide deep ice core WD2014 chronology–Part 1: Methane  
465 synchronization (68–31 ka BP) and the gas age–ice age difference. *Climate of the Past*,  
466 11(2): 153-173, doi:[10.5194/cp-11-153-2015](https://doi.org/10.5194/cp-11-153-2015).
- 467 Burgener, L., Rupper, S., Koenig, L., Forster, R., Christensen, W.F., Williams, J., Koutnik, M.,  
468 Miege, C., Steig, E.J., Tingey, D., Keeler, D., and Riley, L., 2013. An observed negative  
469 trend in Antarctic accumulation rates from 1975 to 2010: Evidence from new observed  
470 and simulated records. *Journal of Geophysical Research-Atmospheres*, 118(10): 4205-  
471 4216.
- 472 Champollion, N., Picard, G., Arnaud, L., Lefebvre, E. and Fily, M., 2013. Hoar crystal  
473 development and disappearance at Dome C, Antarctica: observation by near-infrared  
474 photography and passive microwave satellite. *The Cryosphere*, 7(4): 1247-1262,  
475 doi:[10.5194/tc-7-1247-2013](https://doi.org/10.5194/tc-7-1247-2013).
- 476 Colbeck, S.C., 1982. An overview of seasonal snow metamorphism. *Reviews of Geophysics*,  
477 20(1): 45-61.
- 478 Colbeck, S.C., 1983. Theory of metamorphism of dry snow. *Journal of Geophysical Research:*  
479 *Oceans*, 88(C9): 5475-5482.
- 480 Conger, S.M., McClung, D.M., 2009. Comparison of density cutters for snow profile  
481 observations. *Journal of Glaciology*, 55(189): 163-169.
- 482 Criscitiello, A.S., Das, S.B., Karnauskas, K.B., Evans, M.J., Frey, K.E., Joughin, I., Steig, E.J.,

483 McConnell, J.R., and Medley, B., 2014. Tropical Pacific Influence on the Source and  
484 Transport of Marine Aerosols to West Antarctica. *Journal of Climate*, 27(3): 1343-1363.

485 Das, S.B. and Alley, R.B., 2005. Characterization and formation of melt layers in polar snow:  
486 observations and experiments from West Antarctica. *Journal of Glaciology*, 51(173):  
487 307-312, doi:[10.3189/172756505781829395](https://doi.org/10.3189/172756505781829395).

488 Dash, J.G., Rempel A.W., and Wettlaufer J.S., 2006. The physics of premelted ice and its  
489 geophysical consequences, *Rev. Mod. Phys.* 78, 695-741,  
490 doi:[10.1103/RevModPhys.78.695](https://doi.org/10.1103/RevModPhys.78.695).

491 Fegyveresi, J.M., 2015, Physical properties of the West Antarctic Ice Sheet (WAIS) Divide deep  
492 core: Development, evolution, and interpretation, PhD thesis, The Pennsylvania State  
493 Univ., State College, Pa.

494 Fegyveresi, J.M., Alley, R.B., Fitzpatrick, J.J., Cuffey, K.M., McConnell, J.R., Voigt, D.E.,  
495 Spencer, M.K. and Stevens, N.T., 2016. Five millennia of surface temperatures and ice  
496 core bubble characteristics from the WAIS Divide deep core, West Antarctica.  
497 *Paleoceanography*, 31: 416–433, doi:[10.1002/2015PA002851](https://doi.org/10.1002/2015PA002851).

498 Fitzpatrick, J.J., Voigt, D.E., Fegyveresi, J.M., Stevens, N.T., Spencer, M.K., Cole-Dai, J., Alley,  
499 R.B., Jardine, G.E., Cravens, E.D., Wilen, L.A. and Fudge, T.J., 2014. Physical  
500 properties of the WAIS Divide ice core. *Journal of Glaciology*, 60(224), 1181-1198,  
501 doi:[10.3189/2014JoG14J100](https://doi.org/10.3189/2014JoG14J100).

502 Fukuzawa, T. and Akitaya E., 1993. Depth-Hoar Crystal-Growth in the Surface-Layer under  
503 High-Temperature Gradient. *Annals of Glaciology*, 18: 39-45.

504 Gallet, J.C., Domine, F., Savarino, J., Dumont, M. and Brun, E., 2014. The growth of sublimation  
505 crystals and surface hoar on the Antarctic plateau. *The Cryosphere*, 8(4): 1205-1215,  
506 doi:[10.5194/tc-8-1205-2014](https://doi.org/10.5194/tc-8-1205-2014).

507 Gow, A. 1965. On the accumulation and seasonal stratification of snow at the South Pole. *Journal*  
508 *of Glaciology*, 5(40): 467-477.

509 Gow, A. 1969. On the rates of growth of grains and crystals in south polar firn. *Journal of*  
510 *Glaciology*, 8(53): 241-252.

511 Hammer, C.U., 1985. The influence on atmospheric composition of volcanic eruptions as derived  
512 from ice-core analysis. *Annals of Glaciology*, 7: 125-129.

513 Koerner, R.M. 1971. A stratigraphic method of determining the snow accumulation at Plateau  
514 Station, Antarctica, and application to South Pole-Queen Maud Land traverse 2, 1965-  
515 1966. In Crary, A.P. *Antarctic snow and ice studies II*, (Washington, DC, American  
516 Geophysical Union): 225-238.

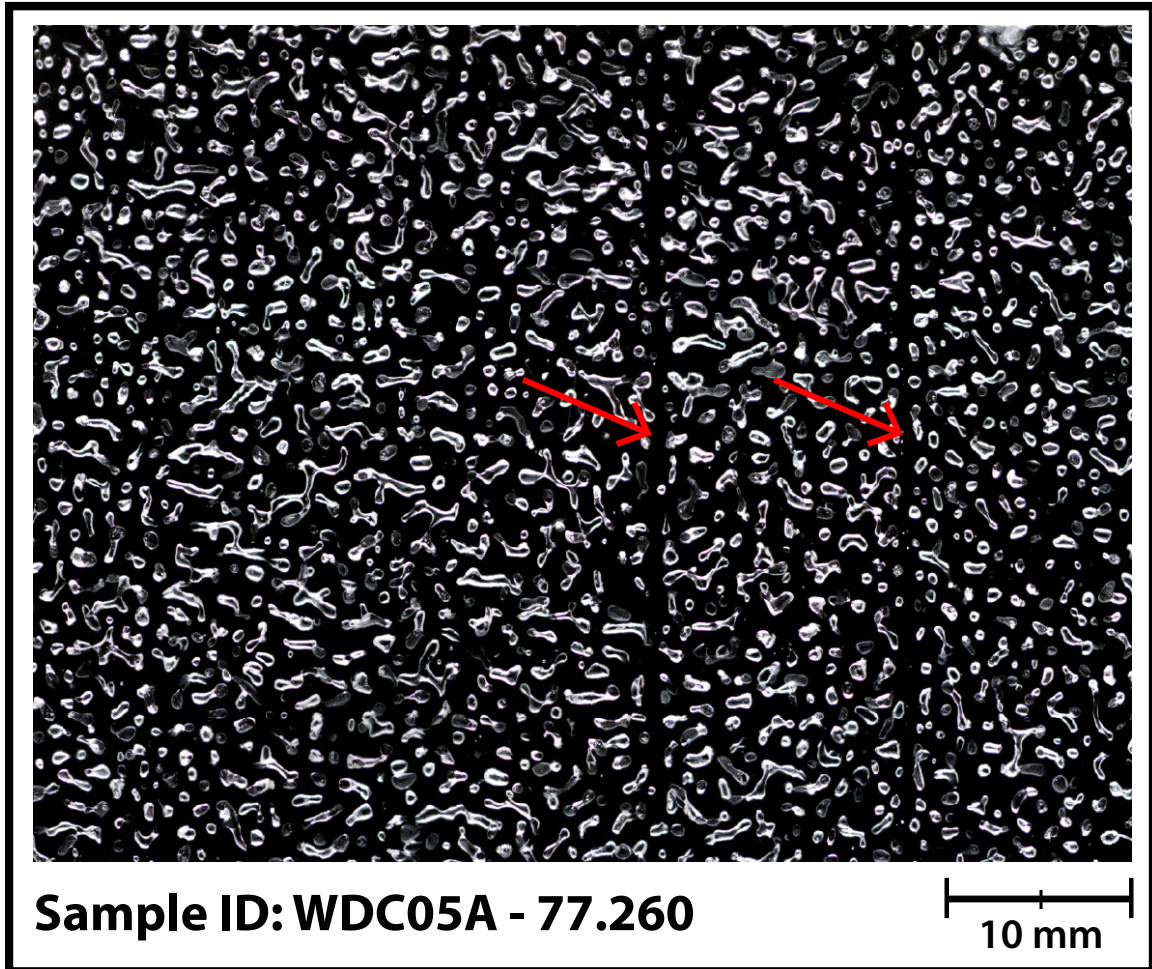
517 Koffman, B.G., Kreutz, K.J., Breton, D.J., Kane, E.J., Winski, D.A., Birkel, S.D., and Kurbatov,  
518 A.V., 2014. Centennial-scale variability of the Southern Hemisphere westerly wind belt  
519 in the eastern Pacific over the past two millennia. *Climate of the Past*, 10(3): 1125-1144.

520 Lazzara, M.A., Weidner, G.A., Keller, L.M., Thom J.E., and Cassano, J.J., 2012. Antarctic  
521 Automatic Weather Station Program 30 Years of Polar Observations. *Bulletin of the*  
522 *American Meteorological Society*, 93(10): 1519-1537, doi:[10.1175/BAMS-D-11-](https://doi.org/10.1175/BAMS-D-11-00015.1)  
523 [00015.1](https://doi.org/10.1175/BAMS-D-11-00015.1).

524 Mitchell, L.E., Buizert, C., Brook, E.J., Breton, D.J., Fegyveresi, J., Baggenstos, D., Orsi, A.,  
525 Severinghaus, J., Alley, R.B., Albert, M. and Rhodes, R.H., 2015. Observing and  
526 modeling the influence of layering on bubble trapping in polar firn. *Journal of*  
527 *Geophysical Research: Atmospheres*, 120(6): 2558-2574, doi:[10.1002/2014JD022766](https://doi.org/10.1002/2014JD022766).

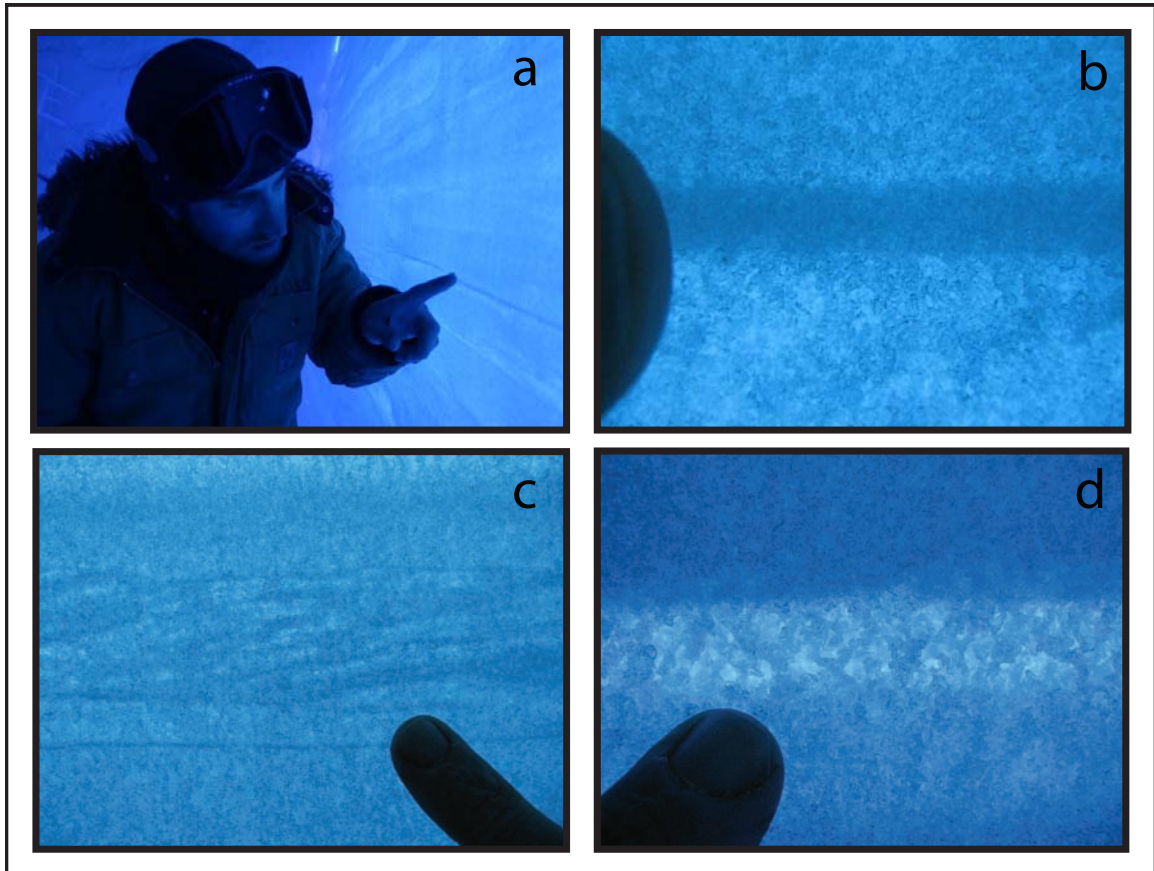
528 Muto, A., Scambos, T.A., Steffen, K., Slater, A.G. and Clow, G.D., 2011. Recent surface  
529 temperature trends in the interior of East Antarctica from borehole firn temperature  
530 measurements and geophysical inverse methods. *Geophysical Research Letters*, 38(15),  
531 doi:[10.1029/2011GL048086](https://doi.org/10.1029/2011GL048086).

- 532 Orsi, A.J., Kawamura, K., Fegyveresi, J.M., Headly, M.A., Alley, R.B. and Severinghaus, J.P.,  
533 2015. Differentiating bubble-free layers from melt layers in ice cores using noble gases.  
534 *Journal of Glaciology*, 61(227): 585-594, doi:[10.3189/2015JoG14J237](https://doi.org/10.3189/2015JoG14J237).
- 535 Sigl, M. et al., 2016. The WAIS Divide deep ice core WD2014 chronology–Part 2: Annual-layer  
536 counting (0–31 ka BP). *Climate of the Past*, 12(3): 769-786, doi:[10.5194/cp-12-769-](https://doi.org/10.5194/cp-12-769-2016)  
537 [2016](https://doi.org/10.5194/cp-12-769-2016).
- 538 Sommerfeld, R.A., 1983. A branch grain theory of temperature gradient metamorphism in snow.  
539 *Journal of Geophysical Research: Oceans*, 88(C2): 1484-1494,  
540 doi:[10.1029/JC088iC02p01484](https://doi.org/10.1029/JC088iC02p01484).
- 541 Sorge, E., 1935. Glaziologische Untersuchungen in Eismitte. *Brockamp, B., and others.*  
542 *Glaziologie. Leipzig, FA Brockhaus*, 935: 62-270.
- 543 WAIS Divide Project Members, 2013. Onset of deglacial warming in West Antarctica driven by  
544 local orbital forcing. *Nature*, 500(7463): 440-444, doi:[10.1038/nature12376](https://doi.org/10.1038/nature12376).
- 545 Weller, G. 1969. The heat and mass balance of snow dunes on the central Antarctic Plateau.  
546 *Journal of Glaciology*, 8: 277-284.  
547  
548



550  
551  
552  
553  
554  
555  
556  
557

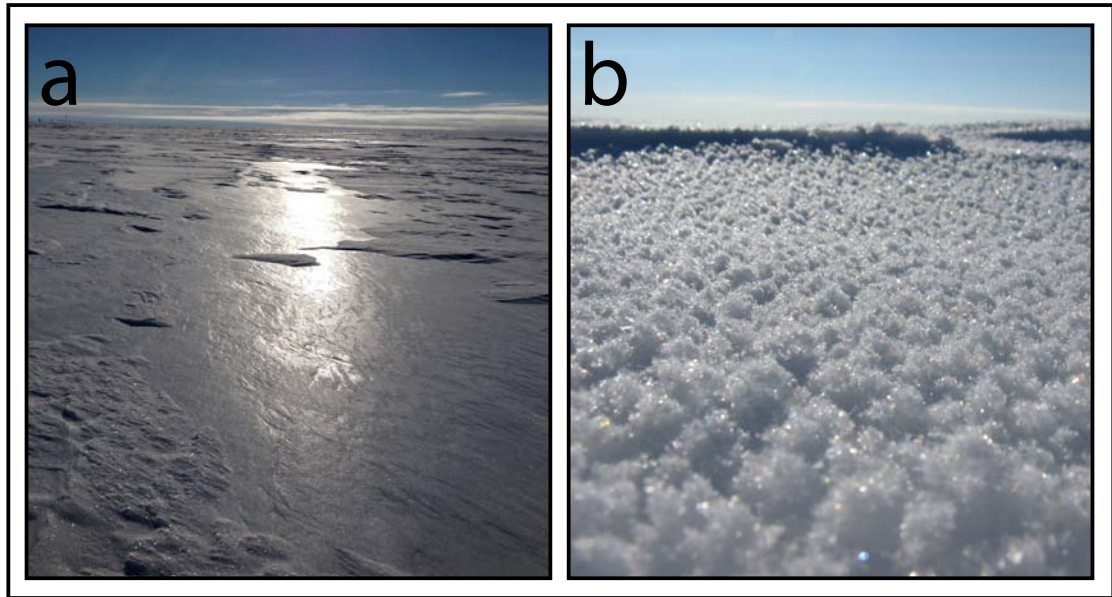
**Figure 1:** A thick-section image of a sample prepared from a depth of ~77.260 meters showing two preserved crusts. Both layers are ~1 mm thick and appear mostly bubble-free. All bubbles here appear white, with the surrounding ice black. The general elongated shape of the bubbles is due the proximity of this sample to the bubble close-off depth at WAIS Divide of ~75 meters). This sample is from the secondary WDC05A core at the WAIS Divide site. Image modified from Orsi et al. [2015].



558  
559  
560  
561  
562

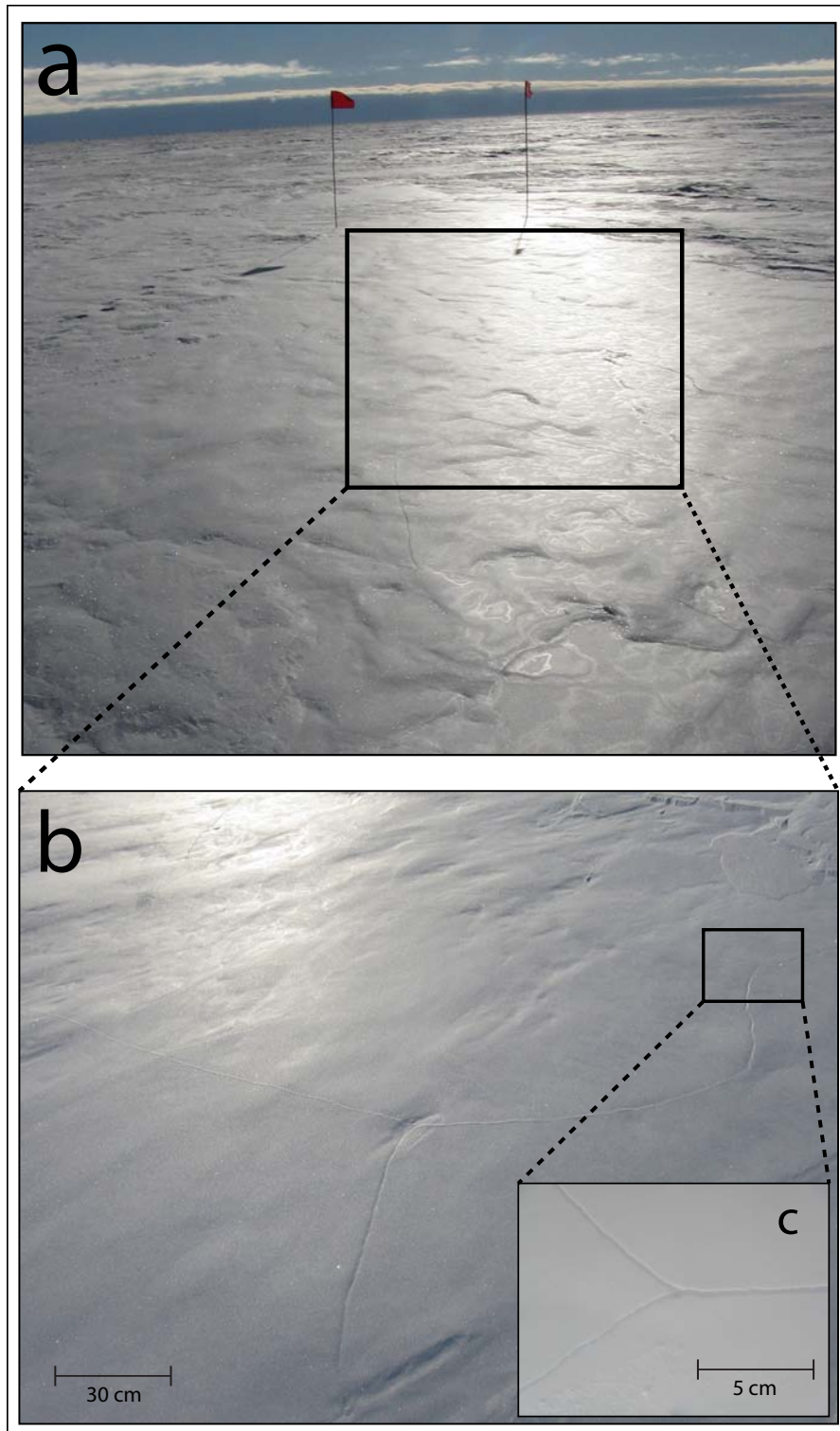
**Figure 2:** The lead author in a 2-meter snow pit prepared at WAIS Divide (pit 2009-10-A). Multi-grain crusts (a, b), preserved sastrugi with cross-bedding (c), and hoar layers (d) are all easily identifiable.





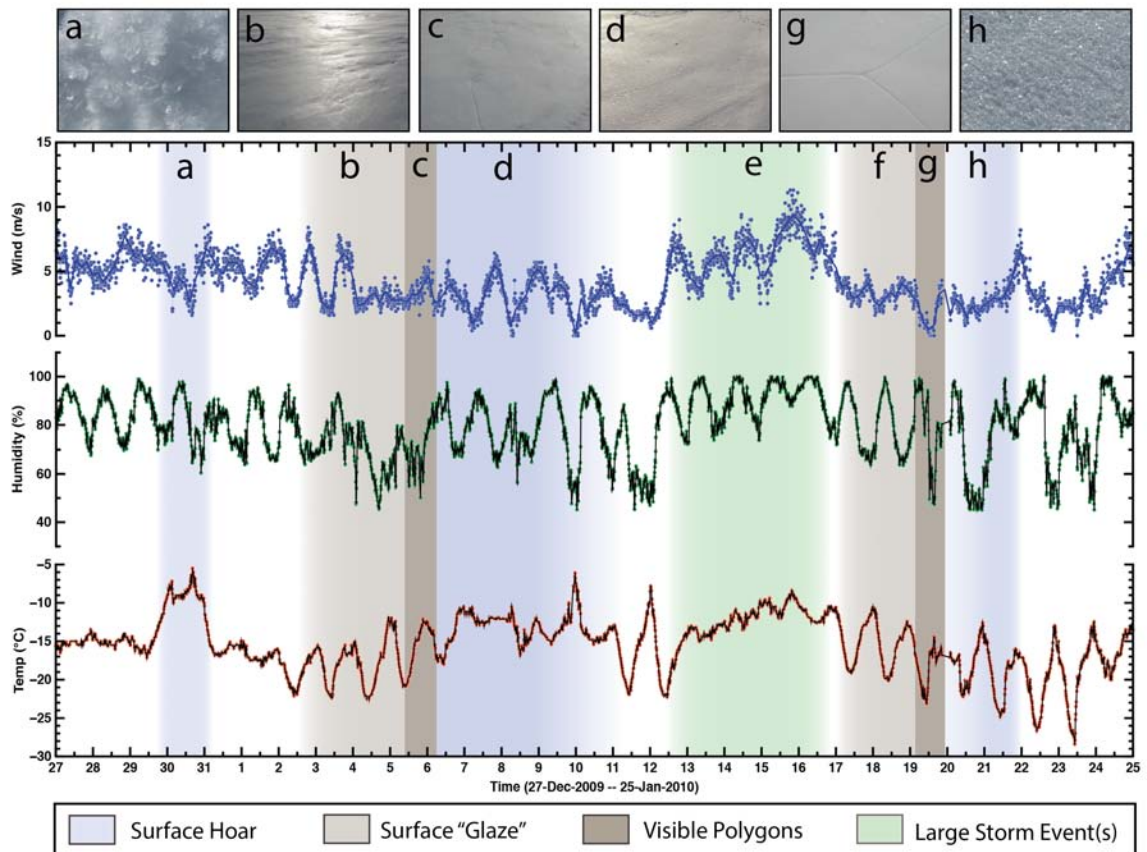
563  
564  
565

**Figure 3:** Surface “glaze” (a) that formed on a calm, sunny day (23-Dec-2012) at WAIS Divide, and the subsequent surface hoar layer (b) that formed on its surface after several calm days.



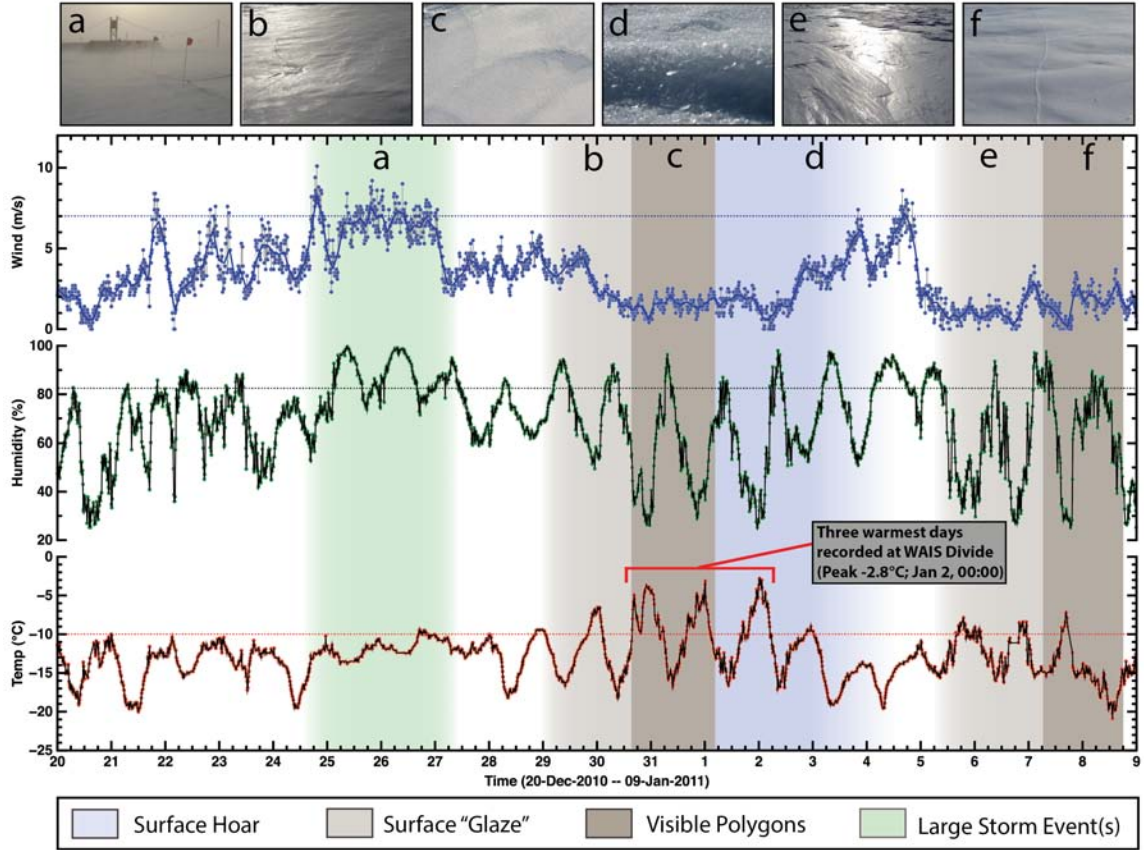
566  
567  
568  
569  
570

**Figure 4:** Surface “glaze” seen at the WAIS Divide site. (a). A zoomed-in view shows the polygonal cracking that initiates at the surface from thermal contraction, following several sunny, clear-sky days (b). Closer inspection reveals greater detail and scale of a crack triple-junction (c).



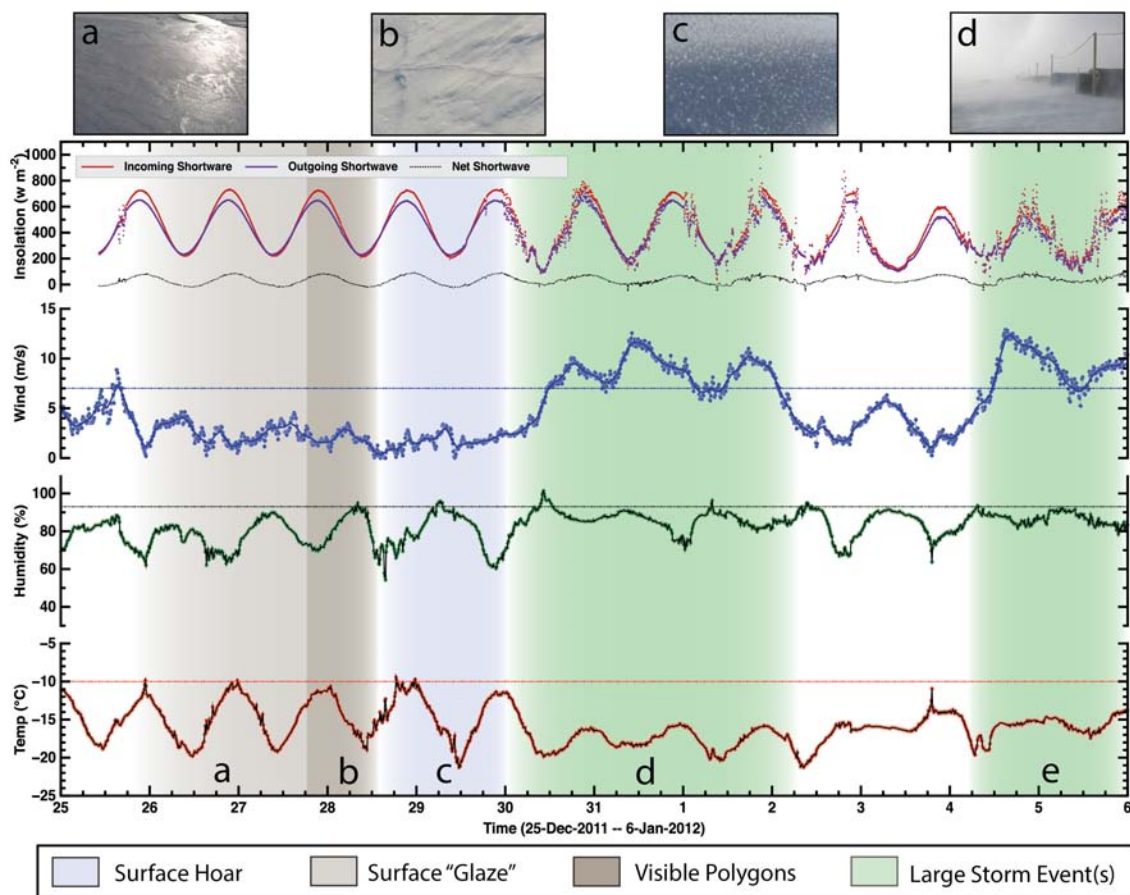
571  
 572  
 573  
 574  
 575  
 576  
 577

**Figure 5:** Surface evolution over 29 days in 2009-10 season, and AWS data. Shading shows episodes of surface hoar, glazes, and polygonal cracking; storm events are also shown. Letters near the top refer to photographs above of specific features or events. All dates and times are GMT (-12 WAIS local time). The errors for all AWS instruments are listed in Supplemental Table S1.



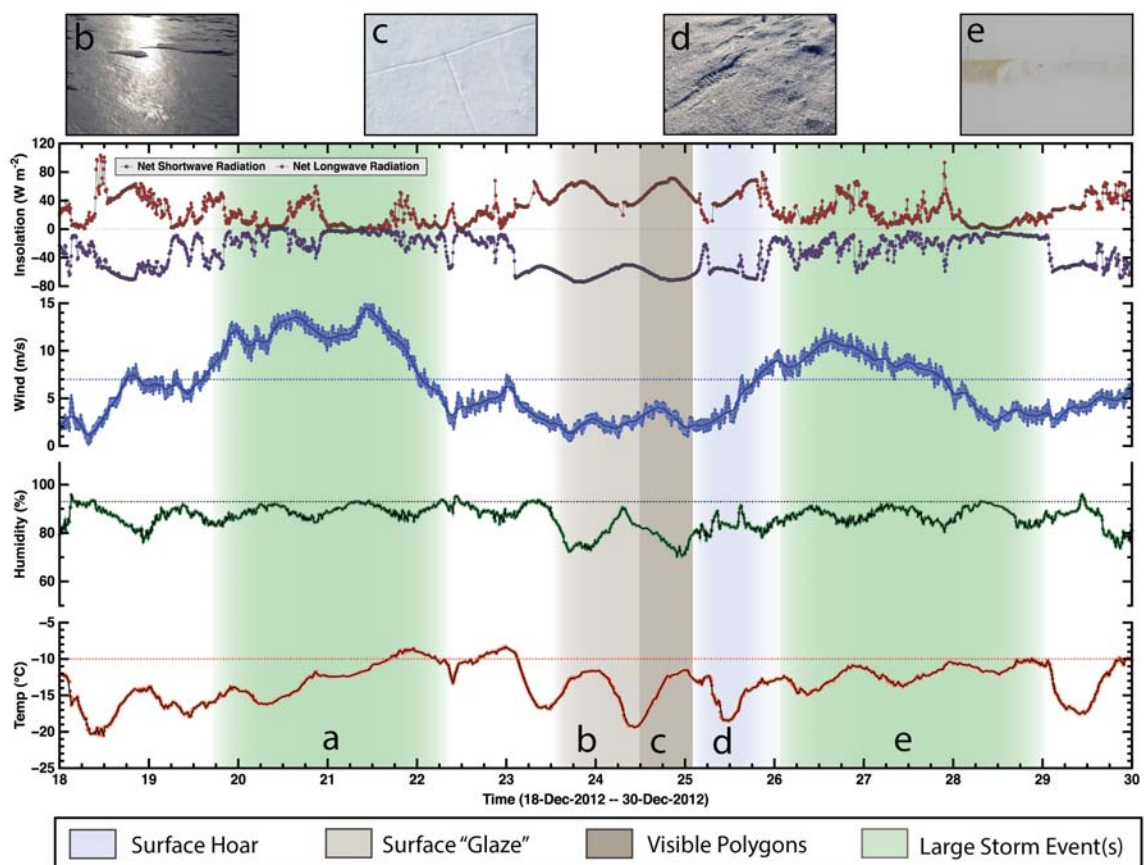
578  
 579  
 580  
 581  
 582  
 583  
 584

**Figure 6:** Surface evolution over 20 days in 2010-11 season, and AWS data. Shading shows episodes of surface hoar, glazes, and polygonal cracking; storm events are also shown. Letters near the top refer to photographs above of specific features or events. All dates and times are GMT (-12 WAIS local time). The errors for all AWS instruments are listed in Supplemental Table S1.



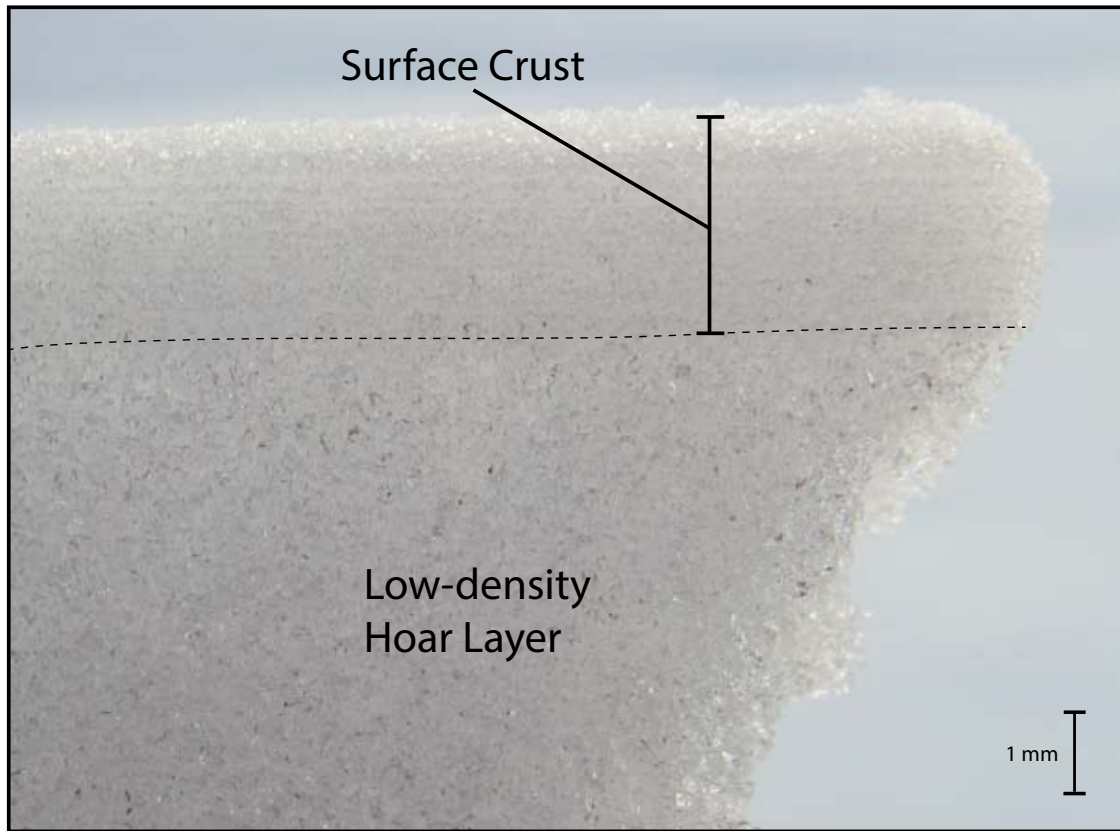
585  
 586  
 587  
 588  
 589  
 590  
 591

**Figure 7:** Surface evolution over 12 days in 2011-12 season, and AWS data. Shading shows episodes of surface hoar, glazes, and polygonal cracking; storm events are also shown. Letters near the top refer to photographs above of specific features or events. All dates and times are GMT (-12 WAIS local time). The errors for all AWS instruments are listed in Supplemental Table S1.



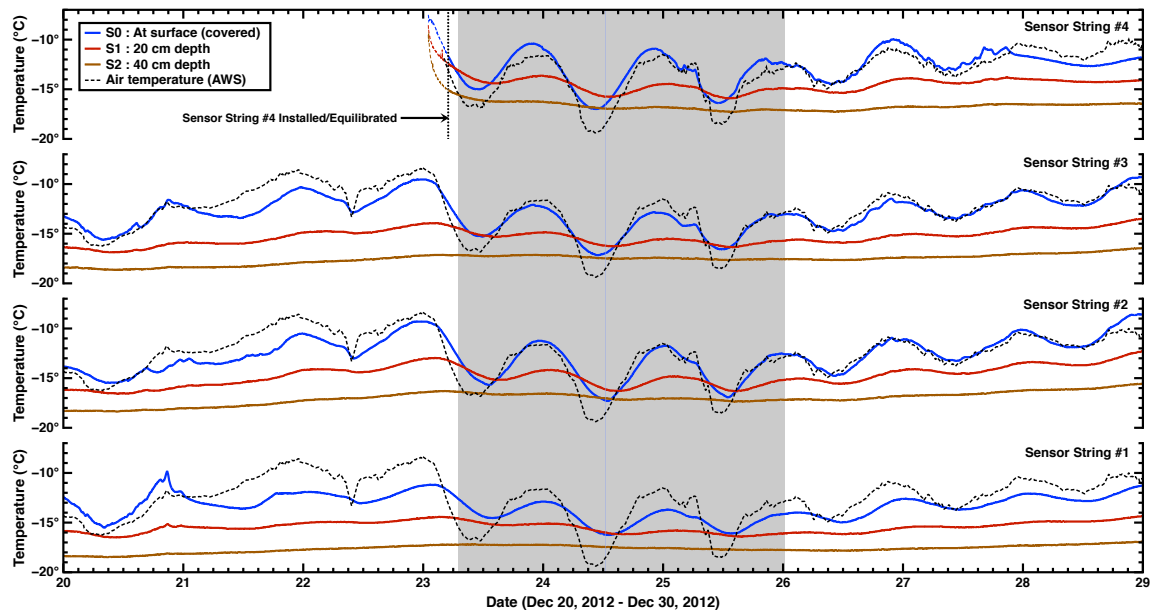
592  
 593  
 594  
 595  
 596  
 597  
 598

**Figure 8:** Surface evolution over 12 days in 2012-13 season, and AWS data. Shading shows episodes of surface hoar, glazes, and polygonal cracking; storm events are also shown. Letters near the top refer to photographs above of specific features or events. All dates and times are GMT (-12 WAIS local time). The errors for all AWS instruments are listed in Supplemental Table S1.



599  
600  
601  
602  
603  
604

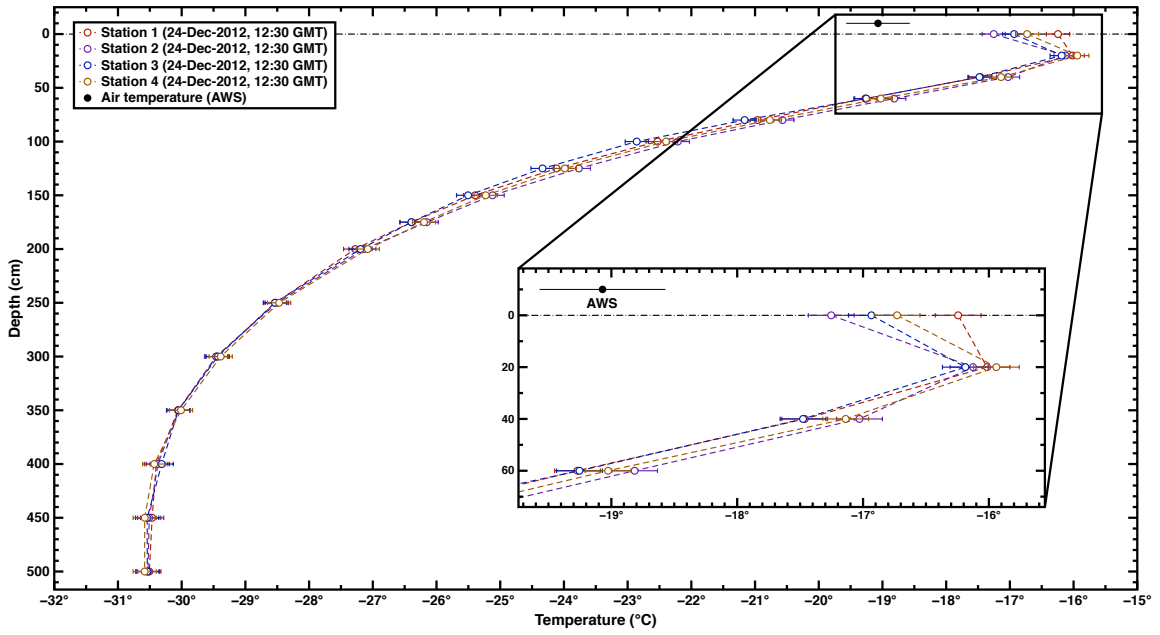
**Figure 9:** A firn sample excavated from a glazed area at WAIS Divide before the onset of polygonal cracking, showing a couplet of an evolved high-density ( $> 400 \text{ kg m}^{-3}$ ),  $\sim 3 \text{ mm}$  multi-grain surface crust containing single-grain crusts, and overlying a lower-density ( $< 300 \text{ kg m}^{-3}$ ) hoar layer.



605  
606

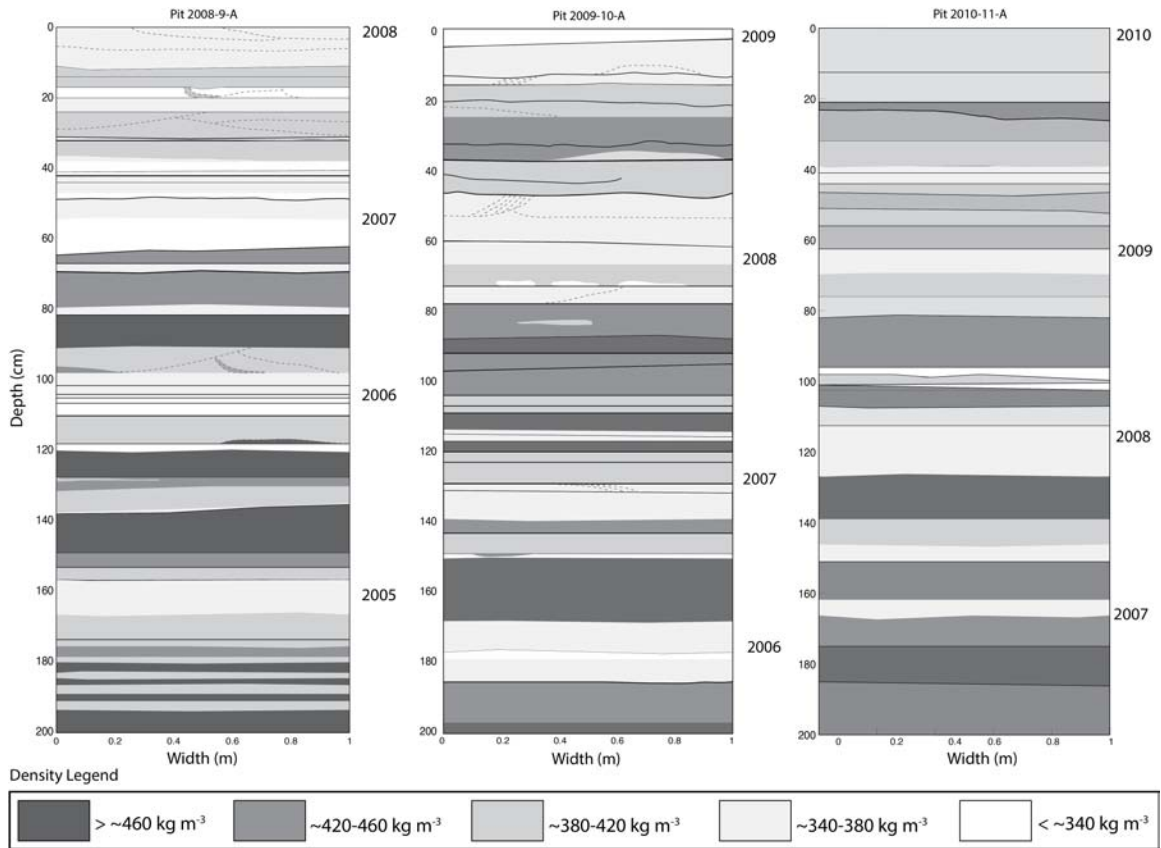
607 **Figure 10:** Temperature measurements (1 min interval) in firn from the 2012-13 season, from the  
 608 upper-most three PRDs (surface down to 40 cm). Data are from the four sensor stations closest to  
 609 the station. The shaded area corresponds to an episode of glaze and hoar growth (see Fig. 8).  
 610 Distinct near-surface temperature inversions occurred each night during this 3-day period (see  
 611 Fig. 11). Sensor #4 was not installed until Dec 22<sup>nd</sup>, and therefore did not equilibrate until early  
 612 on the 23<sup>rd</sup> as indicated. Air temperature is also shown as recorded by the AWS (errors listed in  
 613 Supplemental Table S1). The AWS temperature sensor is located ~1 meter above the snow  
 614 surface. All dates and times are GMT (-12 WAIS local time).





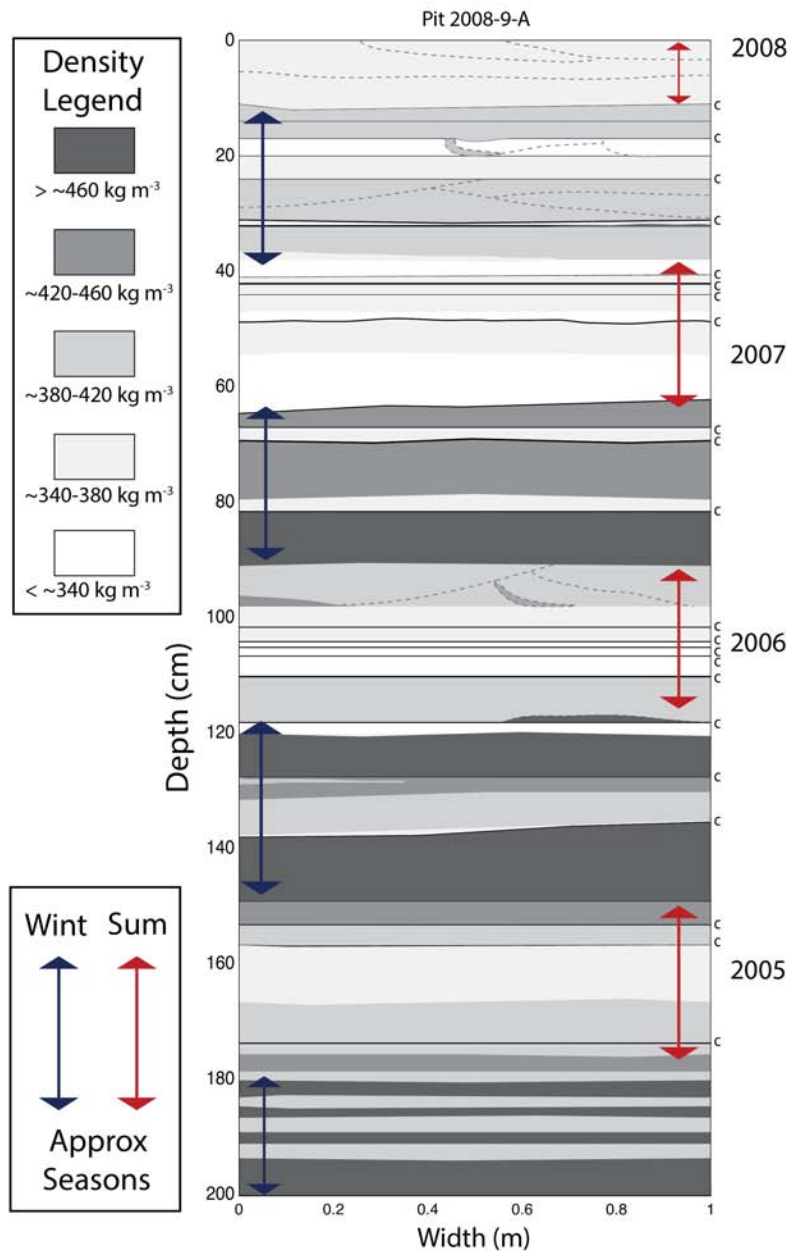
615  
 616  
 617  
 618  
 619

**Figure 11:** Snap-shot temperature readings for PRD-string stations #1-4, taken on 24-Dec-2012 at ~12:30 GMT, showing the temperature inversion with colder air (AWS data) and upper surface air over warmer near-surface firm.



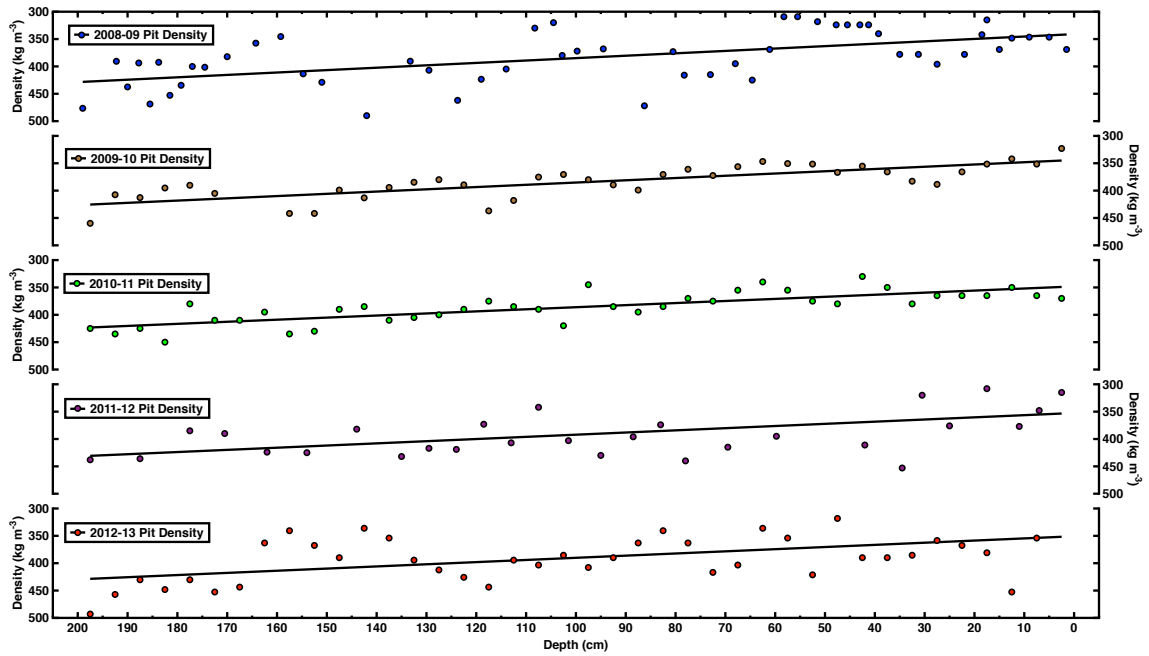
620  
621  
622  
623  
624  
625  
626  
627  
628  
629

**Figure 12:** Complete wall maps of back-lit snow pits prepared during 2008-09, 2009-10, and 2010-11 WAIS Divide field seasons. Layering and density contrast are noted by degree of shading. Fine- to medium- grained, higher-density snow/firn layers are shown with darker grey coloring, whereas coarse-grained and low-density layers (e.g., depth hoar) are shown in white. Crusts are indicated with solid lines, while dotted lines are used to represent cross-bedding at depth. Years were identified based on approximate depths of peak summers and the average measured densities. The pit wall surfaces trend in parallel with the prevailing wind direction at WAIS Divide (approximately north-south, with north to the right).



630  
 631  
 632  
 633  
 634  
 635  
 636  
 637

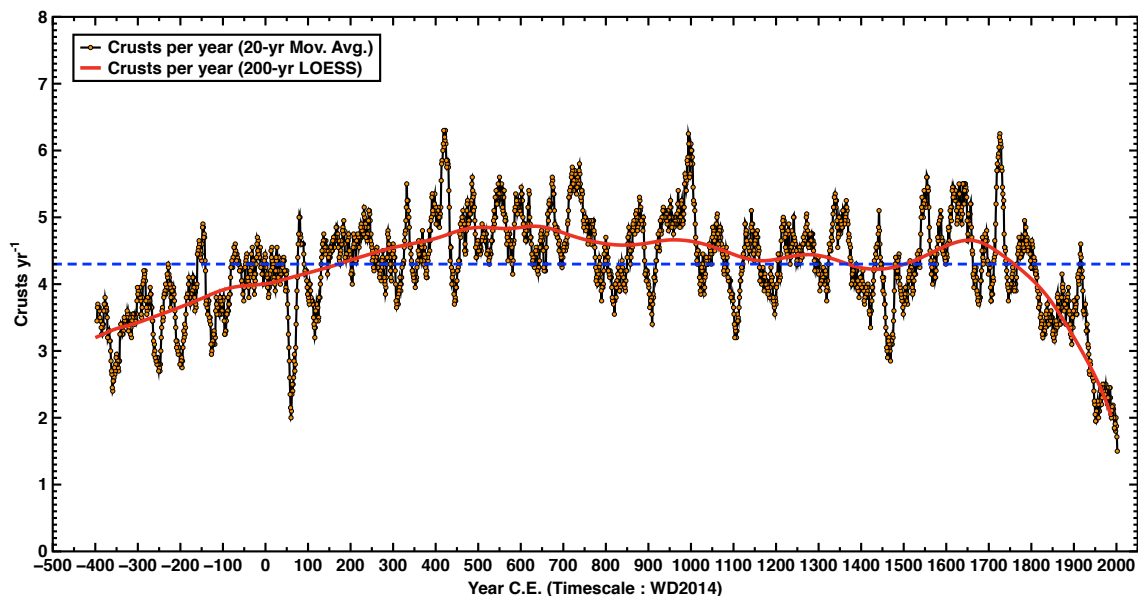
**Figure 13:** A detailed view of data for snow pit 2008-09-A, including wall map, density profile, annual layer picks, and crusts occurrences. Density, layering, and feature preservation are again noted as in Fig. 12. Individual crusts are identified with a labeled “c” along the vertical axis. Seasonal accumulation layers “picked” visually in the pit (shown with red and blue arrows).. These observations indicate a somewhat regular pattern of equally-distributed yearly accumulation at WAIS Divide with clear annual signals.



638  
 639  
 640  
 641  
 642  
 643  
 644

**Figure 14:** Density profiles measured in snow pits from five concurrent seasons at WAIS Divide (2008-2012). Each pit showed a high degree of sample-to-sample variability as measured densities were widely-spaced within the upper 2 meters of firm; estimated annual signals were still identifiable, however. Measurements yielded an overall average density of  $386.6 \pm 3.2 \text{ kg m}^{-3}$  for the upper 2 meters of firm across all 5 pits, with nearly identical linear trend-line slopes of  $\sim 0.4 \text{ kg m}^{-3} \text{ cm}^{-1}$  with depth.

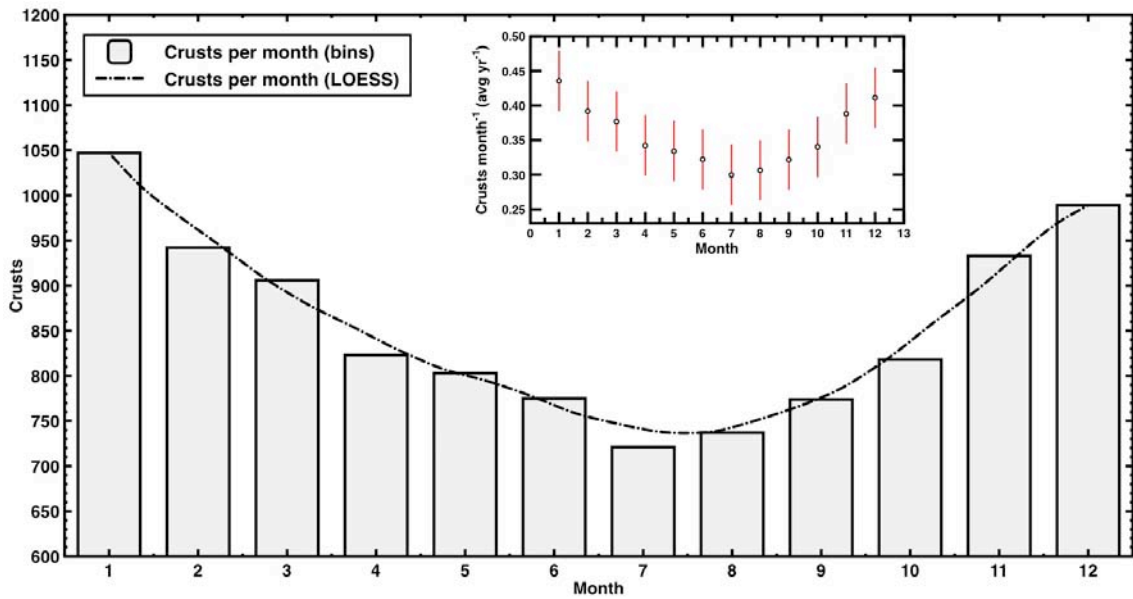
645



646

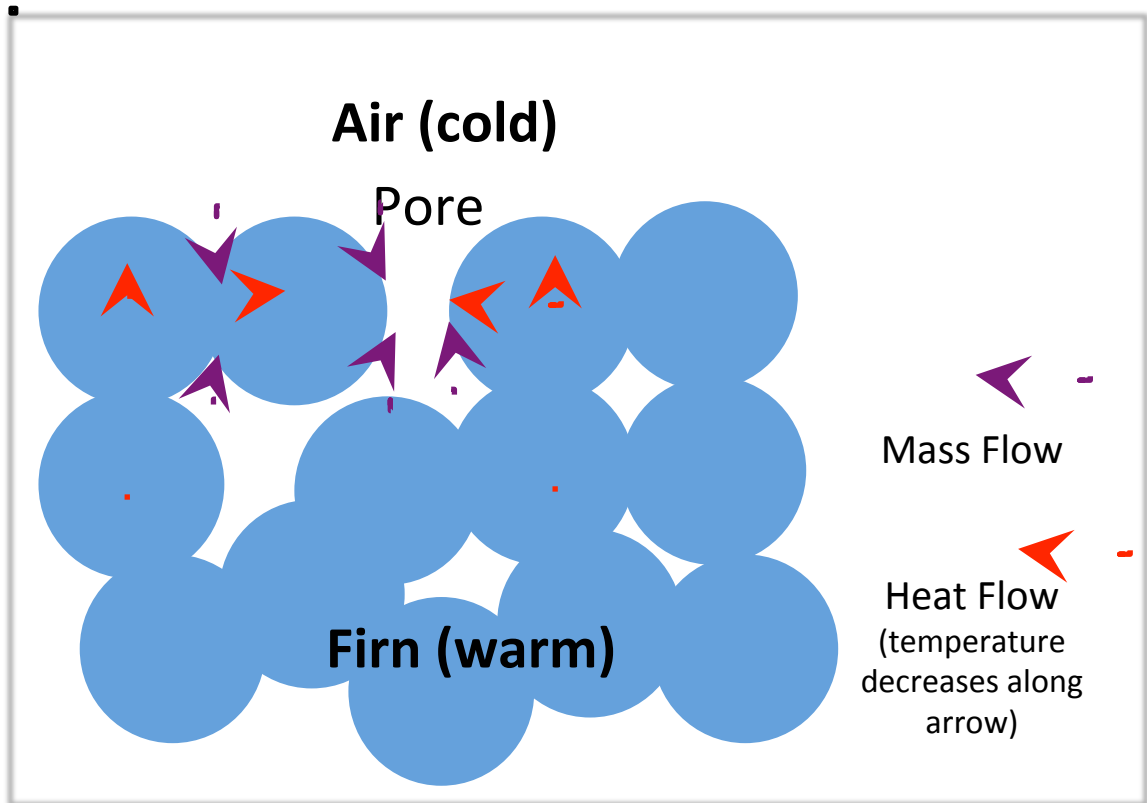
647

648 **Figure 15:** History of crust occurrence (crusts year<sup>-1</sup>) in the bubbly-ice zone of the WDC06A  
649 core that we studied in detail (~120 – 577 m depth); ages (C.E.) are from the WD2014 depth-age  
650 scale). 10,268 unique crusts were documented in the core, for an average rate of  $4.3 \pm 2$  per year  
651 (dashed blue line). Data are shown as 20-yr moving averages for ease of view, with an added 1<sup>st</sup>-  
652 order LOESS smoothing trend-curve (200-yr bin-width). The sharp decline in crust prevalence  
653 after ~1750 C.E. may be due to observational biasing in the shallow firn.



654  
 655  
 656  
 657  
 658  
 659  
 660

**Figure 16:** Crust distribution by month (1=January, 2=February,...12=December) based on assumption that each summer pick in the WD2014 depth-age scale is January 1, and then interpolating linearly. Crusts occur year-round but more commonly in summer accumulation. The smoothed curve is a 1<sup>st</sup>-order LOESS trend curve (width = 2). Data shown for 2400-yr record. Inset shows average crusts per month ( $\pm 1\sigma$ ).



661  
 662  
 663  
 664  
 665  
 666  
 667

**Figure 17:** Schematic illustrating possible mass and heat transports during during formation of a single-grain glazed crust, when the near-subsurface is warmer than the surface. Heat flow is primarily through the grain structure (blue), so pores (white) in the surface layer will be colder than interconnected grains, favoring mass transport from the grains to those pores, increasing density of the surface layer.

668 **Table 1:** Field observation table (see also Figs. 5, 6, 7, 8).

Field Season	Observation Window	Observation Duration	AWS	Other Instrumentation	Pit
2008-2009 <sup>1</sup>	12-Dec-2008 : 10-Jan-2009	~29 days	--	--	x
2009-2010 <sup>1</sup>	27-Dec-2009 : 25-Jan-2010	~29 days	W,H,T	--	x
2010-2011	20-Dec-2010 : 09-Jan-2011	~20 days	W,H,T	--	x
2011-2012 <sup>1</sup>	25-Dec-2011 : 04-Jan-2012	~12 days	W,H,T,I	Dual Li-Cor LI200 sensors Kipp-Zonen CNR2 sensor	x
2012-2013 <sup>1</sup>	18-Dec-2012 : 30-Dec-2012	~12 days	W,H,T,I	Shallow PRD strings <sup>2</sup>	x

W,H,T,I - Wind, Humidity, Temperature, Insolation

<sup>1</sup>Fegyveresi, 2015

<sup>2</sup>Muto et al., 2011

669